npj | climate and atmospheric science

Article

Published in partnership with CECCR at King Abdulaziz University

https://doi.org/10.1038/s41612-025-00906-3

Climate change aggravated wildfire behaviour in the Iberian Peninsula in recent years

Martín Senande-Rivera [1] ✉, Damián Insua-Costa [2] & Gonzalo Miguez-Macho [1]

Climate change is considered to affect wildfire spread both by increasing fuel dryness and by altering vegetation mass and structure. However, the direct effect of global warming on wildfires is hard to quantify due to the multiple non-climatic factors involved in their ignition and spread. By combining wildfire observations with the latest generation of climate models, here we show that more than half of the large wildfires (area>500 ha) occurring in the Iberian Peninsula between 2001 and 2021 present a significant increase in the rate of spread with respect to what it would have been in the pre-industrial period, attributable to global warming. The average acceleration of the rate of spread due to increased fuel dryness is between 2.0% and 8.3%, whereas the influence of enhanced vegetation growth since the pre-industrial period could potentially be even higher than the direct impact of temperature increase in fuel conditions.

Wildfires are an important component of the Earth system continuously interacting with other components such as the atmosphere, vegetation or humans[1–3]. Global fire activity is strongly influenced by climate controls[4,5], and the effects of biomass burning can significantly impact climate by altering the carbon cycle or varying surface albedo[6,7]. Fire regimes are influenced by vegetation patterns or fuel characteristics[8,9] and they can have long-term impacts on forests, plant traits and ecosystem productivity[10–12]. Humans have a direct influence on fire activity, either by igniting fires or by suppressing them[13], and the economic and health impacts of wildfires on society are significant, especially during extreme wildfire events[14,15].

The 6th IPCC Assessment Report (AR6)[16] determines that the likely range of human-induced change in global surface temperature in 2010–2019 relative to 1850–1900 is 0.8 °C to 1.3 °C (due to increases in greenhouse gas concentrations and aerosols, or land-use change), while the likely range of the change attributable to natural forcing is only −0.1 °C to +0.1 °C. In recent years, several studies have shown that this anthropogenic global increase in temperature has led to the intensification of different extreme weather events, such as hurricanes[17,18], heavy precipitation events[19,20], heatwaves[21], or windstorms[22]. Global increases in fire activity have also been linked to ongoing climate change[23–27], but the complex interactions between climate, vegetation and human influences on fire activity mean that these changes are spatially and temporally heterogeneous[28], hampering the application of event attribution methodologies.

When attributing extreme weather events to present climate change, the atmospheric response to anthropogenic forcings can be interpreted as a combination of a thermodynamic and a dynamic component[29]. Regarding wildfires, the thermodynamic component would be associated with the increase in atmospheric water demand (caused by the increased water-holding capacity of a warmer atmosphere), resulting in a general fuel moisture reduction[30,31]. The dynamic component would correspond to the change in the frequency of fire-prone weather patterns, such as those leading to heatwaves or droughts[32,33]. Due to the remaining uncertainties in atmospheric circulation changes induced by global warming[34], we do not quantify the possible dynamic component of climate change influencing fire spread. Since wildfires are not strictly a meteorological event, an additional vegetation-related component must be included. Climate change and atmospheric CO2 fertilization are enhancing vegetation growth[35], which, together with human-induced land-use changes, may increase fuel loads in some regions[36–38], altering wildfire behaviour.

While burned area is increasing in regions like the Western United States[31,39] or Australia[40] as a result of anthropogenic climate change, observed burned area and number of fires have diminished in recent decades in Mediterranean Europe[41], in contrast to the rise in extreme fire weather conditions for this region[42], which is expected to further intensify in the future[43,44]. This observed decrease in burned area is less pronounced in the Iberian Peninsula[41], where some recent extreme events (such as the 2017 and the 2022 fire seasons) have been on an unprecedented scale[45,46].

To understand whether climate change may currently be intensifying extreme wildfires in the Iberian Peninsula, we used the rate of spread to measure the speed at which the fire front advances. Other magnitudes related to wildfire behaviour were also calculated, such as energy release and fire intensity. These magnitudes can be computed from atmospheric and

[1]CRETUS, Non-Linear Physics Group, Universidade de Santiago de Compostela, Santiago de Compostela, Spain. [2]Hydro-Climate Extremes Lab, Ghent University, Ghent, Belgium. ✉e-mail: martin.senande.rivera@usc.es

fuel structure data. We have quantified the increase on the rate of spread attributable to the thermodynamic component of climate change for all wildfires between 2001 and 2021 with a burned area greater than 500 ha. In addition, we analysed how enhanced vegetation growth may have influenced the spread of these wildfires. The comparison between these two contributions is also analysed for a future scenario of intermediate emissions.

Results

Climate change influence on wildfire rate of spread

For each wildfire with a burned area greater than 500 ha between 2001 and 2021 in the Iberian Peninsula, and for each General Circulation Model (GCM), we compare the factual rate of spread (ROS) with the four counterfactual ROS, arising from the two counterfactual periods (pre-industrial and 2070-2099 Shared Socio-economic Pathway 2-4.5, SSP2-4.5) and the two different components of climate change impact (thermodynamic and vegetation growth) considered. From these comparisons we obtain the ROS relative difference for each wildfire (hereafter ROS increase), expressed as a percentage with the factual ROS as the reference. Positive values indicate an increase in ROS over time (i.e. an increase from the pre-industrial period to the present, or from the present to the 2070-2099 SSP2-4.5 period).

Figure 1 shows the probability density function of the obtained relative differences in ROS. Considering the thermodynamic component of climate change, the average ROS increases from preindustrial conditions ranges from 2.0% to 8.3%, depending on the GCM considered, with 4.9% being the mean value of the different models (Fig. 1a). Although the functions depicted in Fig. 1a have their maximum near 0% (representing small changes), they are positively skewed, indicating that some events experienced large ROS increases. A similar pattern, but with larger average ROS increases (between 10.8% and 15.6%, with 12.7% as the mean value), is found for the 2070-2099 SSP2-4.5 future scenario (Fig. 1b). This is in line with the fact that the projected temperature rise for the end of the century is also expected to exceed the current observed warming since pre-industrial conditions (Supplementary Fig. 1). Differences in live fuel moisture show a more important influence on the rate of spread than those in dead fuel moisture, both for the present-past and future-present comparisons (Supplementary Fig. 2).

Fuel load increases due to the greening effect and land use changes (vegetation component of climate change) may have had an even stronger influence (20.7% average ROS increase) from pre-industrial conditions (Fig. 1c). The trends obtained for the vegetation component should be considered as a maximum potential change, as we assume in the

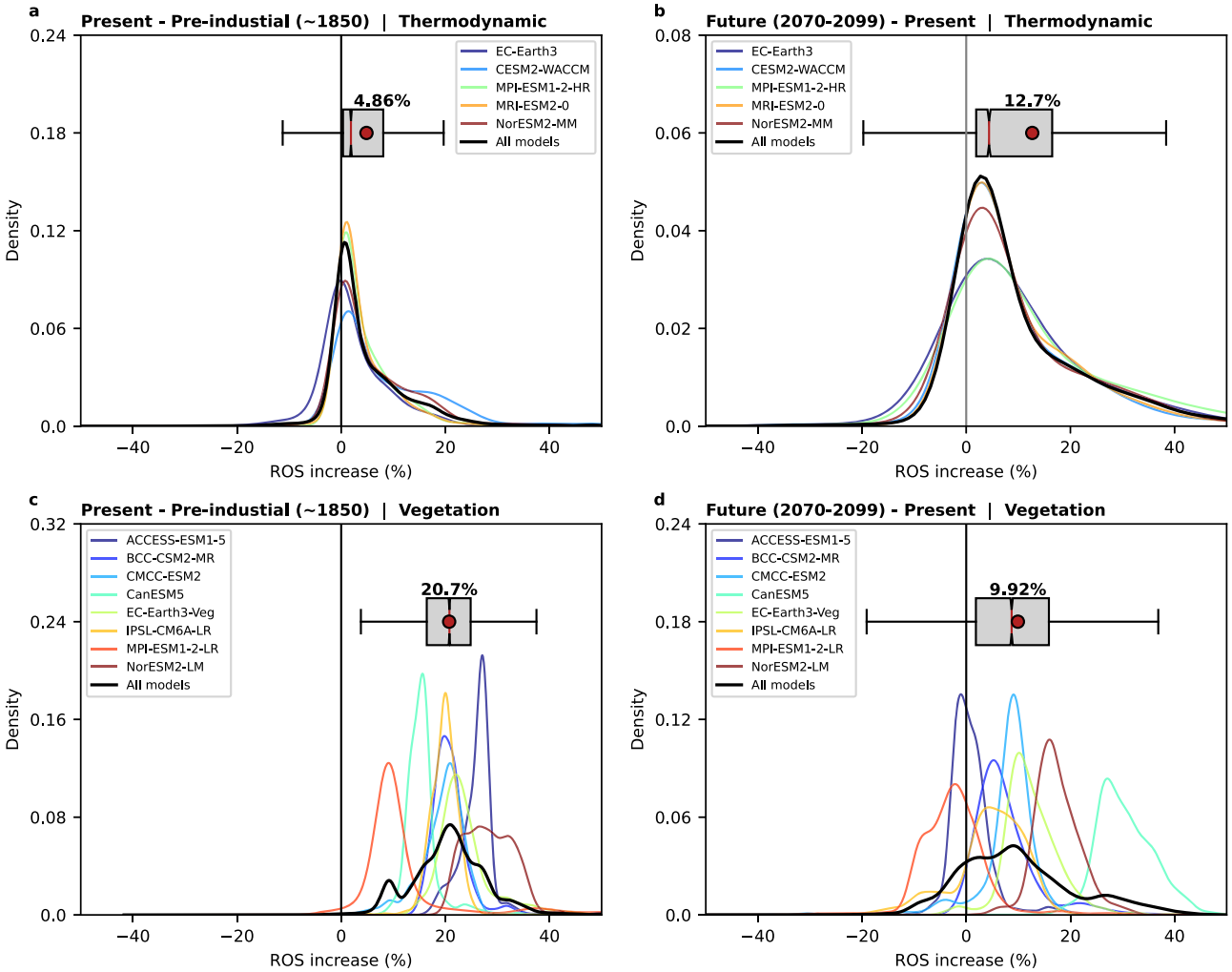

Fig. 1 | ROS increase distributions. Probability density functions of ROS relative differences (ROS increase %) for all wildfires with a burned area greater than 500 ha between 2001 and 2021 in the Iberian Peninsula: **a** considering the thermodynamic component between pre-industrial and present conditions, **b** considering the thermodynamic component between present and 2070-2099 conditions (under SSP2-4.5 scenario), **c** considering vegetation growth component between pre-industrial and present conditions and **d** considering the vegetation growth component between present and 2070-2099 conditions (under SSP2-4.5 scenario). Each colour represents results from a different GCM, and the black line represents all models together. The boxplot also represents the ROS increase distribution for all models, indicating the mean with a red dot and numeric value, and the median with a red line.

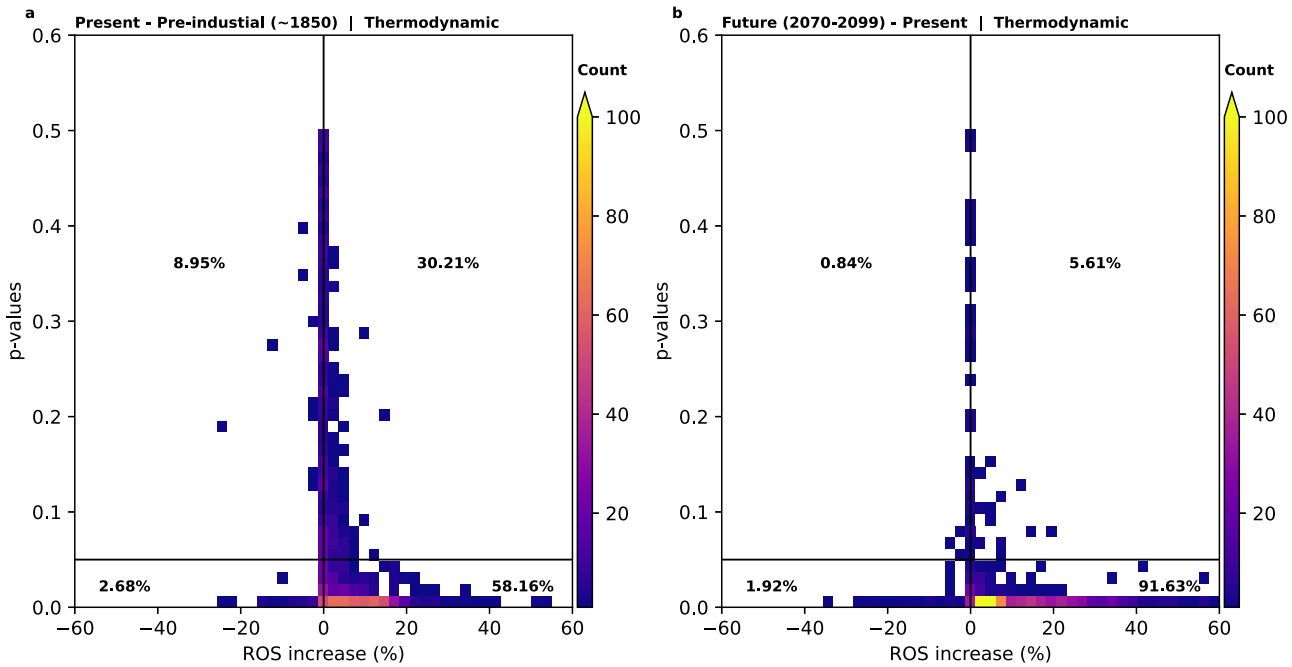

Fig. 2 | Wildfires experiencing significant ROS changes. Bi-dimensional histogram of ROS relative differences (ROS increase %) and *p*-values according to the test for the null-hypothesis that the factual ROS value is equal to the counterfactual ROS model mean. Percentage of wildfires showing a significant (*p*-value < 0.05) and non-significant (*p*-value ≥ 0.05) ROS increase (> 0%) or decrease (< 0%) are showed in each quadrant of the panel. Left panel **a** shows the Present – Pre-industrial comparison, and the right panel **b** shows the Future – Present comparison.

methodology that all gains in net primary productivity translate into a fuel load increase. Part of this potential influence of vegetation modification on the ROS comes from land use change, but it is not the predominant factor (Supplementary Fig. 2). A more moderate average ROS increase (9.92%) is projected for 2070-2099 (Fig. 1d), indicating that wildfire rate of spread increases in the future will be mainly driven by the direct projected temperature rise, rather than by the enhanced vegetation growth.

Nevertheless, the results for the vegetation growth component of climate change present much uncertainty, both for the assumptions we have made in the methodology (we assume that the fuel load increase is proportional to the net primary production gains and that the fuel bulk density is not modified) and for the GCM discrepancies. In addition, our methodology presents an important drawback when analysing this vegetation component in fuel limited regions. Apart from increasing the fuel load, enhanced vegetation growth could also improve fuel continuity[36,37] or modify fuel structures[47], and this could imply that the vegetation growth influence in the ROS could be underestimated in semi-arid regions where fire activity is more constrained by fuel continuity[48] than by fuel mass.

Statistical significance

For each GCM, and considering the thermodynamic component, the T-test is applied for the null hypothesis that 2 related or paired samples (the factual and counterfactual ROS datasets) have identical average values. All models indicate that the means of the two samples are significantly unequal, with *p*-value < 0.01 (Supplementary Table 1). Even if we consider the two samples to be non-related (this would be the case if the two samples contained different fire events, for example when comparing fires from two different time periods), only one model shows a non-significant (*p*-value = 0.172, higher than 0.05) shift of the mean (Supplementary Table 1). This indicates that the difference of the mean of the factual and counterfactual ROS datasets is statistically significant.

The direct influence of the temperature increase in the wildfires' rate of spread (thermodynamic component) is very uneven among different events. We can determine the number of events in which climate change has significantly influenced the rate of spread by using a T-test for the null hypothesis that the factual ROS value of each wildfire is equal to the mean of the counterfactual ROS values (one value per GCM). Among the analysed wildfires, 58% of them have experienced a significant ($p < 0.05$) increase in the rate of spread due to the warming since the pre-industrial period (Fig. 2a). Some of these events, despite showing statistically significant factual-counterfactual differences, their average ROS increments are low (Fig. 2a).

Up to 3% of the wildfires have experienced a significant ROS decrease (Fig. 2a). For the remaining events (39%), the thermodynamic influence of climate change on the rate of spread is non-significant when comparing present against pre-industrial conditions.

When using the 2070-2099 SSP2-4.5 conditions as counterfactual data instead of those of the pre-industrial period, the number of events that undergo a significant ROS increase is much higher (92%). Only 6% of the events show a non-significant result (Fig. 2b).

Climate change influence on other wildfire behaviour parameters

Following the same methodology as for the rate of spread, we calculated the influence of climate change on three United States National Fire Danger Rating System (NFDRS) fire behaviour indices: Spread Component (SC), Energy Release Component (ERC) and Burning Index (BI).

The SC results (Supplementary Fig. 3) are very similar to those of the rate of spread (Fig. 1), as this index also represents how fast fires spread, and the differences in the calculation of SC and ROS are very subtle[49].

The ERC represents the heat per unit area that a wildfire releases to the atmosphere, and it is also influenced by fuel dryness and fuel load changes. The magnitude of the ERC increase is similar to that of the rate of spread when considering the vegetation growth component, both for the present-past (20.7%) and for the future-present (9.9%) comparison (Supplementary Fig. 4). Considering the thermodynamic component of climate change, a slightly lower influence of climate change is found, with an average increase of 3.2% from pre-industrial conditions and 11.7% for the future-present comparison (Supplementary Fig. 4). Similar increments were found for the BI, which is related to flame length and fire intensity[49] (Supplementary Fig. 5).

Spatial and temporal patterns

When analysing the wildfire events separately, a clear spatial pattern emerges for the thermodynamic component of climate change, with large

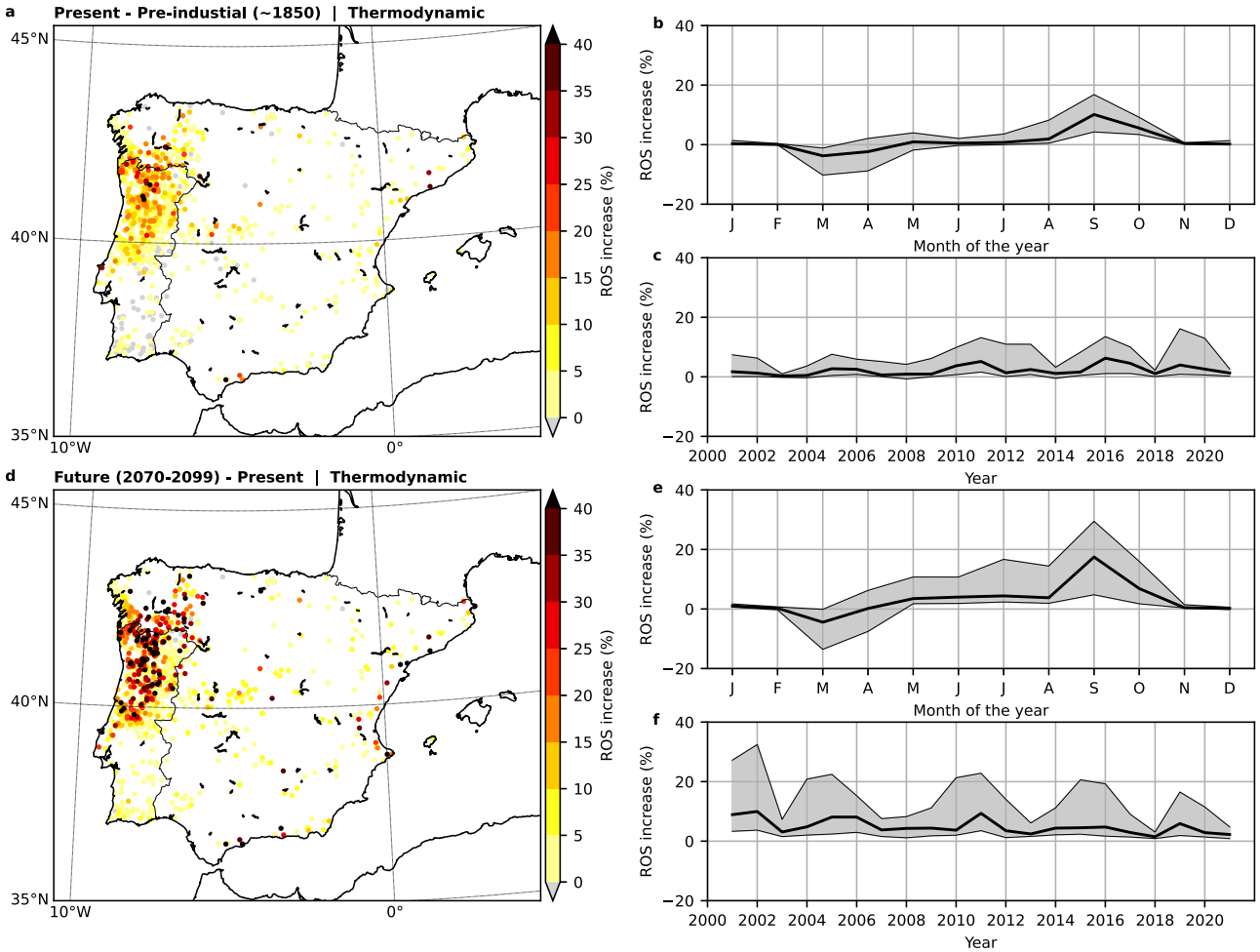

Fig. 3 | Spatial and temporal patterns of ROS changes. ROS increase of each wildfire with a burned area greater than 500 ha between 2001 and 2021 for the Iberian Peninsula considering the thermodynamic component, **a** between pre-industrial and present conditions and **d** between present and 2070-2099 conditions (under SSP2-4.5 scenario). Panels **b** and **c** represent the (**b**) monthly and (**c**) annual distribution of the 25th, 75th and 50th percentiles of the ROS increase of each wildfire between pre-industrial and present conditions, and panels **e** and **f** represent the monthly and annual distributions of the same percentiles between present and 2070-2099 conditions (under SSP2-4.5 scenario).

deviations in its accelerating impact on the ROS among events (Fig. 3). Wildfires in the north of Portugal and the south of Galicia, which is also the region with the highest fire activity at present (hereafter NW region), show the most significant variation in ROS for both the past-present and present-future comparisons, with individual increases of up to 50% (Fig. 3a, d).

As we only analyse fires that have actually occurred, the spatial and temporal patterns shown in Fig. 3 may have a certain bias, since they may be correlated. To avoid this issue and understand the causes behind these patterns, we calculated the 100-h dead fuel moisture content (DFMC) and the herbaceous live fuel moisture content (LFMC) for all points in the domain and all days of the analysed period, regardless of whether a wildfire had taken place or not, as proxies for the ROS change (Fig. 4). A similar pattern to that of ROS increase arises in this comparison, with the north of Portugal and the south of Galicia displaying the most significant fuel moisture reductions (Fig. 4). Moreover, in the NW region the two contributions, DFMC and LFMC, are temporally synchronised, with the maximum fuel moisture reduction occurring at the end of the summer (from August to September), leading to an amplification of the total ROS increase during a time of the year with high fire activity. In contrast, in the south of the Iberian Peninsula the two contributions do not result in the maximum fuel moisture reduction in the same months, thus their combined impact on the ROS is smaller.

Regarding the temporal distribution of the ROS changes, we observe that the most pronounced increases occur at the end of the summer (Fig. 3b, e). In general, during these months we find the most important reductions in moisture content for both dead and live fuels (Fig. 4b, d). In the case of dead fuels, this is due to a greater concatenation of dry days, where fuel moisture is predominantly determined by temperature and humidity. In the case of live fuels, it is explained by the fact that the vapour pressure deficit commonly exceeds 900 Pa during these months (Supplementary Fig. 6), a value at which the vegetation stomata begin to close affecting moisture content[50]. Live fuel's behaviour also explains the observed ROS reductions at the end of the winter (Fig. 3e), when the rise of the minimum temperature can enhance photosynthesis and anticipate the start of the vegetation growing season, leading to higher live fuel moisture and lower ROS.

Looking at the ROS changes by year, we see that the increases from the pre-industrial past are larger for the most recent fires (Fig. 3c), and that the expected changes in the future are larger for the oldest fires (Fig. 3f). This is a sign that the temperature has already been rising during the 2001–2021 period.

Discussion

We conclude from the results that the fires that have taken place in recent years in the Iberian Peninsula have developed under environmental conditions that are more favourable for their spread than would be the case in a climate unaltered by anthropogenic greenhouse gas emissions. Most of the increase found in the ROS of recent fires comes from changes in vegetation rather than from those in atmospheric thermodynamic conditions. For the

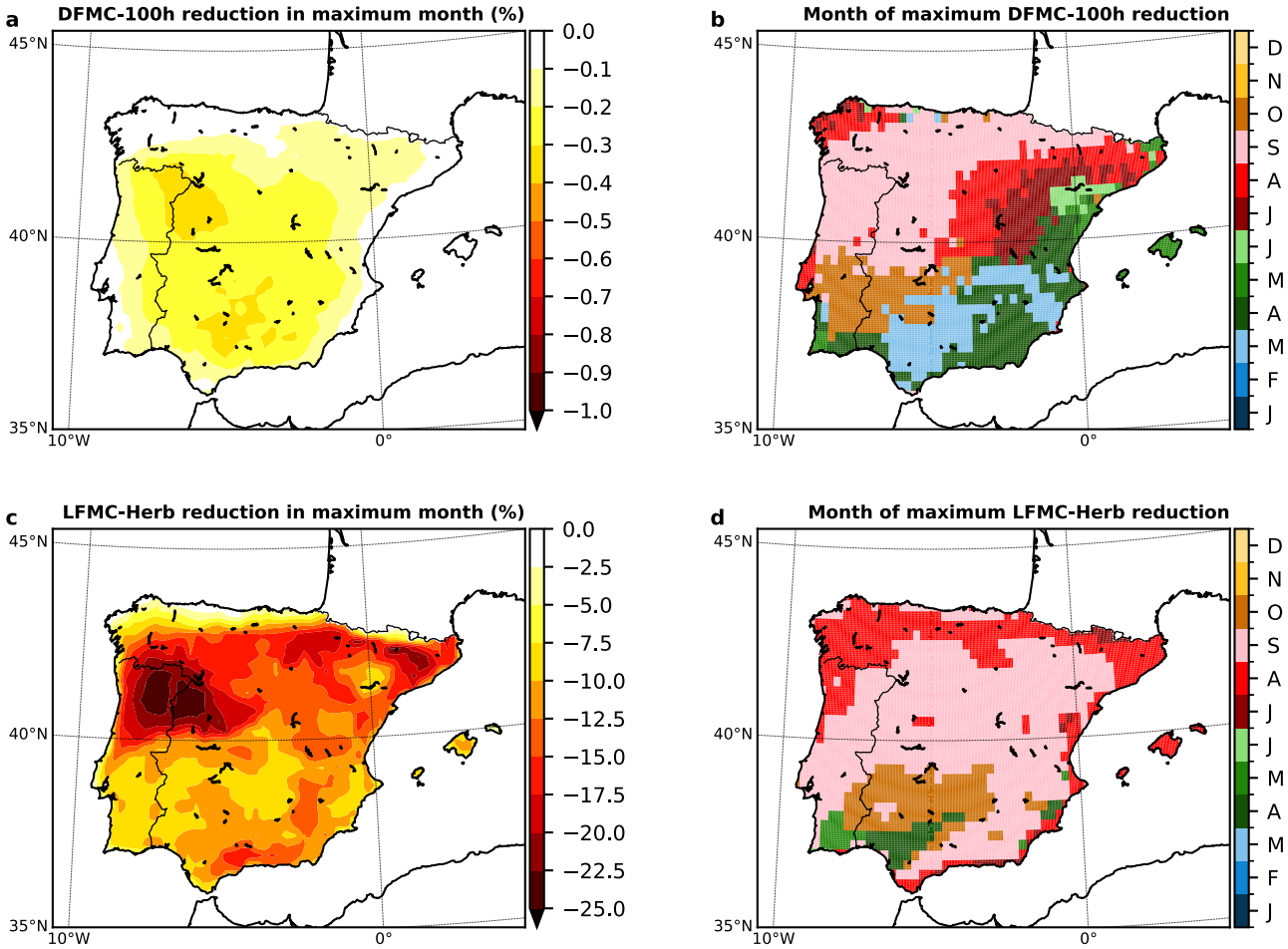

Fig. 4 | Spatial and temporal patterns of fuel moisture changes. For all grid points, from pre-industrial to present conditions, **a** 100-h dead fuel moisture changes (DFMC) during the month of maximum fuel moisture reduction on average, **b** month of maximum 100-h dead fuel moisture reduction on average, **c** herbaceous live fuel moisture changes (LFMC) during the month of maximum fuel moisture reduction on average and **d** month of maximum herbaceous live fuel moisture reduction on average.

future, the relevance of both contributions reverse. While accelerated global warming enhances the thermodynamic impact on the ROS, the changes arising from alterations in vegetation growth show a pattern in which present-future ROS increases are less pronounced than past-present increases (Fig. 1c, d). This is due to the fact that vegetation greening is controlled by several factors such as atmospheric CO2 fertilization, vegetation-related climatic drivers (changes in temperature or precipitation that enhance vegetation growth), nitrogen deposition and land-use changes[35,51], the combined effect of which could result in a nonlinear relation between vegetation greening and global warming. For instance, in semi-arid or low productivity regions (such as the south of the Iberian Peninsula), the conjunction of the predicted warming and precipitation reduction could aggravate the water deficit and counterbalance the effect of CO2 fertilization in vegetation productivity[35,51].

Previous studies have shown an overall increase in fire risk for the Iberian Peninsula[25,27,42,52,53]. However, here we analysed the extent to which climate change may have affected, not fires in a broad sense, but the particular fires that have already occurred in the region, which in turn can provide valuable information for understanding the relation between climate change and fires in general. To assess the conditions under which the fires actually recorded spread, we chose parameters specifically related to fire spread characteristics, such as the ROS or the energy released, rather than fire danger indices such as the Canadian Fire Weather Index. The latter are used to determine more generally whether weather conditions are favourable for fire occurrence, from ignition to spread[54,55], and are not so directly linked to the particulars of individual events.

The 6th IPCC Assessment Report (AR6)[16] mentions the limited number of attribution studies of compound events such as fires. With this type of studies, we can better understand how climate change affects these events, which are influenced by interactions between different elements such as meteorology, humans or vegetation. We believe that this approach based on event attribution allows us to better understand the complexity of the relationship between climate change and fires, since, as we have seen, this relationship is highly case-dependent, with significant temporal and spatial variability. Moving from the more common approach of fire weather analysis to that of event attribution may also help to better understand the contradicting trends between increasing fire weather and decreasing burned area in some regions.

The ROS of a fire is related to the area burned, but the connection is not straightforward. The fact that one fire has a higher ROS than another does not necessarily mean that it will burn more hectares. The final area burned is determined by a complex development, involving non-environmental factors, such as orography or means of control and suppression[1,9]. For this reason, it is difficult to interpret the increase in ROS in terms of burned area, especially in a region where the authorities try to control and extinguish most fires[56]. What we can infer is that the relation is non-linear, and that in cases of a very significant increase in the ROS, the fire could overwhelm the capacity of the authorities to control it[57,58], generally resulting in a significant expansion of the area burned.

We thus argue that the fires where the increase in ROS is highest (the right tails of the probability distributions in Fig. 1) are likely to be those where climate change may have had a significant influence on burned area.

In contrast, for fires where the increase in ROS is close to 0% (a large number considering the thermodynamics component, Fig. 1a) the influence of climate change on burned area is likely small.

The region of the Iberian Peninsula where warming has the largest impact on fire spread conditions is the inland northwest, which in turn is the area with the highest fire activity in recent years (Fig. 2a, d). In addition, the months of the year with the greatest influence are months of very high fire activity as well, toward the end of the dry summer, especially August, September and October (Fig. 2b, e).

This spatio-temporal distribution can also have an amplifying effect on burned area due to the potential for simultaneous occurrence of fires, all with enhanced ROS. When multiple fires occur at the same time and in the same area, suppression and control resources are more easily overwhelmed[58–61], which can lead to an increase in the area burned.

The probabilistic distributions of changes in heat release and in fire intensity due to global warming (Supplementary Figs. 4 and 5) also have pronounced rightward tails indicating very high increases for some events. A large increase in released energy and fire intensity suggests that fires have a greater ability to alter atmospheric conditions, creating convective updrafts that can lead to the development of pyroconvective clouds (pyrocumulonimbus or pyroCb)[62–66]. Fires with deep pyroconvection have a chaotic behaviour, governed by strong updrafts and downdrafts, which can make control and suppression tasks more difficult[67–71] and also result in an important enlargement of the area burned, as is the case with highly accelerated ROS.

Several studies suggest an increase in fire danger or burned area in the Iberian Peninsula due to climate change in the future[30,43,44,72,73]. One would expect that the area burned would have been progressively expanding in recent years, along with the recorded warming[74–76]. However, no significant positive trend is observed in either the total burned area or the number of fires between 1980 and 2021 (Supplementary Fig. 7). In fact, the trend in burned area is negative, although not statistically significant. This can be seen as a paradox: increasingly favourable conditions for fire spread but no increase in burned area.

Two factors could explain this paradox. The first is the improvement in suppression efforts that occurred in this period (1980–2021)[41,77,78], with the introduction of measures such as early intervention with aerial means or fire lighting prevention[79]. The second is the increase in the percentage of area burned by large fires (over 500 ha, 1000 ha and 5000 ha) (Supplementary Fig. 8). Firefighting may have been very effective in reducing the impact of most fires, but not enough for those for which global warming has a more intense enhancing effect, or for some of those occurring simultaneously in the areas of highest activity in the northwest, as we discussed above. This is in line with Cunningham et al.[80], who pointed out that although global burned area may be decreasing, fire behaviour is worsening. This increase in the relative importance of large fires supports the idea developed in this section that the relation between conditions for fire spread and burned area is non-linear: although conditions are increasingly favourable for spread, the increase in burned area is mostly restricted to the most intense fires that exceed control and suppression capacity.

Extreme fires had major social, economic and ecological impacts on the Iberian Peninsula. The socio-economic impacts include direct fatalities[45], fire smoke health effects[81,82] and economic losses due to damages on human assets[59]. Ecological impacts include degradation of forest ecosystems[83] and even marine ecosystems due to the deposition of ash and sediments in the water[84], which in turn lead to economic losses in the forestry and shellfish industries. Based on the results of this study, the socio-economic and ecological impacts of fires are expected to increase in the future due to anthropogenic climate change. Adaptive and transformative-resilience actions would be required in order to guarantee a sustainable coexistence with wildfire[85], such as vegetation management to reduce fire severity, transformation of the built environment to minimize severe fire's impacts or accepting fire-caused shifts in ecological systems[86].

Methods

Fire and climate data

We created a database of wildfires with a burned area greater than 500 ha occurring between 2001 and 2021 in the Iberian Peninsula by combining data from Portuguese and Spanish public institutions. The Portuguese data come from the Forest Fire Information Management System (Sistema de Gestão de Informação de Incêndios Florestais, SGIF), which is part of the Institute for Nature and Forests Conservation (Instituto da Conservação da Natureza e das Florestas, ICNF). The data, that can be downloaded here (https://www.icnf.pt/florestas/gfr/gfrgestaoinformacao/estatisticas), and includes information about the location (in coordinates), date of ignition and burned area of individual fires from 2001. The Spanish data come from the General Forest Fire Statistics (Estadística General de Incendios Forestales, EGIF), produced by the Ministry of Ecological Transition and Demographic Challenge (Ministerio de Transición Ecológica y Reto Demográfico, MITECO). The data, which can be downloaded here (https://www.miteco.gob.es/gl/biodiversidad/temas/incendios-forestales/estadisticas-datos.html), includes information about the location (in coordinates), date of ignition and burned area of individual fires from 1968. We cross-checked this data with the list of >500 ha wildfires in the annual reports produced by the same institution, which also includes information about the location, date of ignition and burned area. In the Spanish fire database, some fires do not have an exact location in coordinates, but only the municipality where they originated. For these cases, we have approximated the location by the centroid of the polygon of the corresponding municipality (NUTS5), using the centroid algorithm of the QGIS software. The database contains information about the location, date of ignition and burned area of 1365 wildfires.

Present climate data were obtained from the ERA5 database[87], the fifth generation ECMWF (European Centre for Medium-Range Weather Forecasts) reanalysis for the global climate, which combines model data with observations. To analyse the climate change thermodynamic influence on fire behaviour, we used the Coupled Model Intercomparison Project Phase 6 CMIP6 historical, pre-industrial and future projections from 5 general circulation models (GCMs): MPI-ESM1-2-HR, EC-Earth3, CESM2-WACCM, MRI-ESM2-0 and NorESM2-MM. The pre-industrial control simulation (piControl) is performed under conditions chosen to be representative of the period prior to the onset of large-scale industrialization, with 1850 being the reference year. We used the "middle of the road" Shared Socio-economic Pathway 2-4.5 (SSP2-4.5), reflecting an intermediate emissions pathway leading to a nominal 4.5 $W{\cdot}m^{-2}$ radiative forcing level by 2100[88,89]. For each model, we only consider the main ensemble member (r1i1p1f1). Only these 5 models provide the needed variables under the three experiments considered (piControl, historical and SSP2-4.5) at high resolution. For the analysis of the vegetation component, we used 8 GCMs modelling net primary production (NPP): ACCESS-ESM1-5, BCC-CSM2-MR, CMCC-ESM2, CanESM5, EC-Earth3-Veg, IPSL-CM6A-LR, MPI-ESM1-2-LR and NorESM2-LM. Apart from piControl, historical and SSP2-4.5 experiments, we also used the hist-noLu experiment: a historical simulation that is identical to the CMIP6 historical concentration-driven simulation, except that land use is held constant with pre-industrial values[90]. This experiment allows us to quantify the influence of land-use changes in wildfire behaviour. There is no equivalent experiment for future scenarios (i.e. future-emissions simulations but using historical land-use data), so the land-use contribution cannot be identified when assessing the influence of projected vegetation growth on fire rate of spread. Only these 8 models provide the NPP variable for the three experiments considered (piControl, historical, hist-noLu and SSP2-4.5).

Rate of spread calculation

Fire rate of spread (ROS) is computed using the Rothermel's surface fire spread model[49,91]. These equations were obtained by considering that energy is conserved at the fire front[49,91]. The final equation states that the rate of spread is equal to the ratio of the heat flux absorbed by the fuel that is not yet burning (I_P) to the product of the effective mass of this fuel (ρ_{be}) and the

energy that a unit mass needs to burn (Q_{ig}).

$$ROS = \frac{I_P}{\rho_{be} \cdot Q_{ig}}$$

The full model needs 5 inputs: the moisture content of dead fuels, the moisture content of live fuels, surface wind speed, terrain slope and some structure-related fuel properties (specified in different fuel models).

Surface wind speed is directly obtained from climatological data, and the slope factor is neglected in this study, since it is not affected by climate change. Fuel moisture content values (for both live and dead fuels) were calculated following the 2016 version of the United States National Fire Danger Rating System (NFDRS2016) procedures. Dead fuel moisture content (DFMC) values were obtained with Nelson's fuel moisture model[92], a physics-based model that calculates heat and moisture transfer between the fuel interior and the environment by using finite-difference numerical methods, with 2 m temperature, total precipitation, relative humidity and solar radiation as input variables. The model was run with hourly weather data, using a 1-month period of spin-up for each fire. Model parameters for different size fuels were obtained from the literature[93]. Live fuel moisture contents (LFMC) were calculated through the Growing Season Index[50], which considers daylength, vapour pressure deficit and minimum temperatures to predict foliar phenology. We tested the performance of this index by comparing the resulting moisture contents with some in-situ observations of live fuel moisture contents in Spain[94] (Supplementary Fig. 9).

The fuel models used in this study were obtained from the 1-km European fuel database produced by Aragoneses et al.[95]. These models, based on the 40 Scott and Burgan fuel models[96], are descriptions of different representative fuel types, in terms of morphologic characteristics. We assigned to each fire the most abundant fuel model in the fire area (within a 60 km radius from the fire reference location). A quantification of possible alterations of the main results by the selection of this 60 km radius is shown in the "Fuel selection distance test" of the Supplementary Information.

To avoid unrealistic ROS values, we have excluded fires from the analysis where the fuel moisture is higher or close to the fuel moisture of extinction (the moisture content of a specific fuel type above which a fire will not propagate), $(FMC - FMC_{ext})<1\%$. This reduces the fire database to 1195 fires instead of the original 1365 fires. More information about this, and a quantification of possible alterations of the main results by the selection of this threshold value can be consulted in the "Fuel moisture threshold test" section of the Supplementary Information.

In addition, we also calculated other indexes related to wildfire behaviour from NFDRS2016: Spread Component (SC), Energy Released Component (ERC) and the Burning Index (BI). The Spread Component is also an estimation of the rate of spread (with very small differences in their calculation compared to the Rothermel's ROS equations[49]), the Energy Released Component represents the heat per unit area released by the fire, and the Burning Index is related to flame length and fire intensity[49].

Attribution method

For each of the analysed wildfires we obtain one factual ROS obtained from ERA5 reanalysis climate data, and several counterfactual rates of spread. The latter correspond to the two counterfactual periods (pre-industrial and 2070-2099 SSP2-4.5) and to the two different components of climate change (the thermodynamic component and the vegetation growth component) that we analysed. We used five GCMs for the thermodynamic component and eight GCMs for the vegetation component (which is the number of models that provide the variables and experiments we need); therefore, we compute 26 different counterfactual rates of spread for each wildfire.

Counterfactual rates of spread for the thermodynamic component experiment are obtained by perturbing the thermodynamic variables of the factual ERA5 dataset. Ten perturbed climate datasets are needed: five representing pre-industrial conditions (one for each GCM) and five representing 2070-2099 conditions (according to the SSP2-4.5 scenario). Inspired by the pseudo-global-warming approach[97,98], counterfactual datasets are obtained according to the following expression:

$$X_{counterfactual} = X_{factual} + \left(X^{GCM}_{counterfactual} - X^{GCM}_{factual}\right)$$

Here, $X_{counterfactual}$ indicates a value of the counterfactual dataset for a given location and time, $X_{factual}$ is the corresponding value of the factual dataset (ERA5), $X^{GCM}_{counterfactual}$ is the corresponding monthly value averaged over the counterfactual period of each GCM and $X^{GCM}_{factual}$ is the corresponding monthly value averaged over a 30-year centred window in the historical period of each GCM. Since CMIP6 historical data extends up to 2014, we use the future scenario of intermediate emissions (SSP2-4.5) to cover the entire period we are analysing (2001–2021). The $\left(X^{GCM}_{counterfactual} - X^{GCM}_{factual}\right)$ anomaly, which was obtained from monthly data, is then interpolated in time to daily data.

Since we focus on the thermodynamic component of climate change, no dynamics-dependent variables such as surface wind speed or total precipitation are perturbed. We only change temperature-related variables (2 m temperature, daily maximum temperature, daily minimum temperature and 2 m dew point temperature).

The two inputs to the ROS computation that are directly affected by the perturbation of the thermodynamic variables are the DFMC and LFMC. We calculate these two quantities, and from them the ROS for each wildfire event, from factual and counterfactual data, obtaining a reference value corresponding to factual conditions, plus five values (one for each GCM) for pre-industrial conditions, and five values (again, one for each GCM) for 2070-2099 SSP2-4.5 conditions.

Changes in the thermodynamic environment, but also in precipitation, CO2 fertilization, nitrogen deposition or land use, would also impact the ROS of wildfires by altering vegetation structure as well as mass, i.e., the amount of available fuel. We refer to the impact on the latter as the vegetation growth component of climate change, and we quantify it by simply perturbing the total fuel load of each fuel model. For that purpose, we first obtain a greening/browning factor by dividing the mean annual NPP of the considered counterfactual period by the mean annual NPP of the corresponding 30-year centred window in the historical period (extended with SSP2-4.5 data). We then multiply the total fuel amount of each fuel model by this factor. The procedure is the same as for the thermodynamic variables, except that we now use a multiplicative factor (instead of adding an anomaly), since the variable we modify in the equations (fuel load) is not the same as the one we get from the global models (NPP). We assume that this variation of fuel load occurs while keeping the amount of fuel per volume (bulk density) constant, hence an idealized approach. This assumption implies that our results (when analysing the vegetation growth component) must be considered as a maximum potential change of the rate of spread. As mentioned above, NPP data was available from eight different GCMs for analysis.

Data availability

The data that support the findings of this study is available in this Harvard Dataverse repository (https://doi.org/10.7910/DVN/EN4QVP).

Code availability

The code used to analyse and produce the data that support the findings of this study is available in this Harvard Dataverse repository (https://doi.org/10.7910/DVN/EN4QVP).

Received: 25 May 2024; Accepted: 3 January 2025;
Published online: 15 January 2025

References

1. Bowman, D. M. et al. Vegetation fires in the Anthropocene. *Nat. Rev. Earth Environ.* **1**, 500–515 (2020).

2. Flannigan, M. D., Krawchuk, M. A., de Groot, W. J., Wotton, B. M. & Gowman, L. M. Implications of changing climate for global wildland fire. *Int. J. Wildland Fire* **18**, 483–507 (2009).
3. Bowman, D. M. et al. Fire in the Earth system. *Science* **324**, 481–484 (2009).
4. Marlon, J. R. et al. Climate and human influences on global biomass burning over the past two millennia. *Nat. Geosci.* **1**, 697–702 (2008).
5. Senande-Rivera, M., Insua-Costa, D. & Miguez-Macho, G. Spatial and temporal expansion of global wildland fire activity in response to climate change. *Nat. Commun.* **13**, 1208 (2022).
6. Turetsky, M. R. et al. Global vulnerability of peatlands to fire and carbon loss. *Nat. Geosci.* **8**, 11–14 (2015).
7. Randerson, J. T. et al. The impact of boreal forest fire on climate warming. *Science* **314**, 1130–1132 (2006).
8. Archibald, S., Lehmann, C. E., Gómez-Dans, J. L. & Bradstock, R. A. Defining pyromes and global syndromes of fire regimes. *Proc. Natl Acad. Sci.* **110**, 6442–6447 (2013).
9. Kelley, D. I. et al. How contemporary bioclimatic and human controls change global fire regimes. *Nat. Clim. Change* **9**, 690–696 (2019).
10. Bowd, E. J., Banks, S. C., Strong, C. L. & Lindenmayer, D. B. Long-term impacts of wildfire and logging on forest soils. *Nat. Geosci.* **12**, 113–118 (2019).
11. Harrison, S. P. et al. Understanding and modelling wildfire regimes: an ecological perspective. *Environ. Res. Lett.* **16**, 125008 (2021).
12. Pellegrini, A. F. et al. Fire frequency drives decadal changes in soil carbon and nitrogen and ecosystem productivity. *Nature* **553**, 194–198 (2018).
13. Andela, N. et al. A human-driven decline in global burned area. *Science* **356**, 1356–1362 (2017).
14. Johnston, F. H. et al. Estimated global mortality attributable to smoke from landscape fires. *Environ. Health Perspect.* **120**, 695–701 (2012).
15. Bowman, D. M. et al. Human exposure and sensitivity to globally extreme wildfire events. *Nat. Ecol. Evol.* **1**, 0058 (2017).
16. IPCC. Climate Change 2021: The Physical Science Basis. Contribution of Working Group I to the Sixth Assessment Report of the Intergovernmental Panel on Climate Change. vol. In Press (2021).
17. Reed, K. A., Stansfield, A. M., Wehner, M. F. & Zarzycki, C. M. Forecasted attribution of the human influence on Hurricane Florence. *Sci. Adv.* **6**, eaaw9253 (2020).
18. Reed, K. A., Wehner, M. F. & Zarzycki, C. M. Attribution of 2020 hurricane season extreme rainfall to human-induced climate change. *Nat. Commun.* **13**, 1905 (2022).
19. Eden, J. M., Wolter, K., Otto, F. E. L. & Oldenborgh, G. J. Multi-method attribution analysis of extreme precipitation in Boulder, Colorado. *Environ. Res. Lett.* **11**, 124009 (2016).
20. Eden, J. M. et al. Extreme precipitation in the netherlands: an event attribution case study. *Weather Clim. Extrem.* **21**, 90–101 (2018).
21. Philip, S. Y. et al. Rapid attribution analysis of the extraordinary heat wave on the Pacific coast of the US and Canada in June 2021. *Earth Syst. Dyn.* **13**, 1689–1713 (2022).
22. González-Alemán, J. J. et al. Anthropogenic Warming Had a Crucial Role in Triggering the Historic and Destructive Mediterranean Derecho in Summer 2022. *Bull. Am. Meteorol. Soc.* **104**, E1526–E1532 (2023).
23. Jolly, W. M. et al. Climate-induced variations in global wildfire danger from 1979 to 2013. *Nat. Commun.* **6**, 7537 (2015).
24. Abatzoglou, J. T., Williams, A. P., Boschetti, L., Zubkova, M. & Kolden, C. A. Global patterns of interannual climate–fire relationships. *Glob. Change Biol.* **24**, 5164–5175 (2018).
25. Ellis, T. M., Bowman, D. M., Jain, P., Flannigan, M. D. & Williamson, G. J. Global increase in wildfire risk due to climate-driven declines in fuel moisture. *Glob. Change Biol.* **28**, 1544–1559 (2022).
26. Liu, Z., Eden, J. M., Dieppois, B. & Blackett, M. A global view of observed changes in fire weather extremes: uncertainties and attribution to climate change. *Clim. Change* **173**, 14 (2022).
27. Jones, M. W. et al. Global and regional trends and drivers of fire under climate change. *Rev. Geophys.* **60**, e2020RG000726 (2022).
28. Williams, A. P. & Abatzoglou, J. T. Recent advances and remaining uncertainties in resolving past and future climate effects on global fire activity. *Curr. Clim. Change Rep.* **2**, 1–14 (2016).
29. Shepherd, T. G. et al. Storylines: an alternative approach to representing uncertainty in physical aspects of climate change. *Clim. Change* **151**, 555–571 (2018).
30. Clarke, H. et al. Forest fire threatens global carbon sinks and population centres under rising atmospheric water demand. *Nat. Commun.* **13**, 7161 (2022).
31. Williams, A. P. et al. Observed impacts of anthropogenic climate change on wildfire in California. *Earths Future* **7**, 892–910 (2019).
32. Ruffault, J. et al. Increased likelihood of heat-induced large wildfires in the Mediterranean Basin. *Sci. Rep.* **10**, 13790 (2020).
33. Turco, M. et al. On the key role of droughts in the dynamics of summer fires in Mediterranean Europe. *Sci. Rep.* **7**, 1–10 (2017).
34. Shepherd, T. G. Atmospheric circulation as a source of uncertainty in climate change projections. *Nat. Geosci.* **7**, 703–708 (2014).
35. Zhu, Z. et al. Greening of the Earth and its drivers. *Nat. Clim. Change* **6**, 791–795 (2016).
36. Wu, M. et al. Sensitivity of burned area in Europe to climate change, atmospheric CO2 levels, and demography: a comparison of two fire-vegetation models. *J. Geophys. Res. Biogeosciences* **120**, 2256–2272 (2015).
37. Pausas, J. G. & Keeley, J. E. Wildfires and global change. *Front. Ecol. Environ.* **19**, 387–395 (2021).
38. Allen, R. J., Gomez, J., Horowitz, L. W. & Shevliakova, E. Enhanced future vegetation growth with elevated carbon dioxide concentrations could increase fire activity. *Commun. Earth Environ.* **5**, 1–15 (2024).
39. Turco, M. et al. Anthropogenic climate change impacts exacerbate summer forest fires in California. *Proc. Natl Acad. Sci.* **120**, e2213815120 (2023).
40. Canadell, J. G. et al. Multi-decadal increase of forest burned area in Australia is linked to climate change. *Nat. Commun.* **12**, 6921 (2021).
41. Turco, M. et al. Decreasing fires in mediterranean Europe. *PLoS One* **11**, e0150663 (2016).
42. Giannaros, T. M., Kotroni, V. & Lagouvardos, K. Climatology and trend analysis (1987–2016) of fire weather in the Euro-Mediterranean. *Int. J. Climatol.* **41**, E491–E508 (2021).
43. Turco, M. et al. Exacerbated fires in Mediterranean Europe due to anthropogenic warming projected with non-stationary climate-fire models. *Nat. Commun.* **9**, 3821 (2018).
44. Calheiros, T., Pereira, M. & Nunes, J. P. Assessing impacts of future climate change on extreme fire weather and pyro-regions in Iberian Peninsula. *Sci. Total Environ.* **754**, 142233 (2021).
45. Turco, M. et al. Climate drivers of the 2017 devastating fires in Portugal. *Sci. Rep.* **9**, 13886 (2019).
46. Rodrigues, M. et al. Drivers and implications of the extreme 2022 wildfire season in Southwest Europe. *Sci. Total Environ.* **859**, 160320 (2023).
47. Teckentrup, L. et al. Response of simulated burned area to historical changes in environmental and anthropogenic factors: a comparison of seven fire models. *Biogeosciences* **16**, 3883–3910 (2019).
48. Pausas, J. G. & Paula, S. Fuel shapes the fire–climate relationship: evidence from Mediterranean ecosystems. *Glob. Ecol. Biogeogr.* **21**, 1074–1082 (2012).
49. Andrews, P. L. *The Rothermel Surface Fire Spread Model and Associated Developments: A Comprehensive Explanation*. (2018).
50. Jolly, W. M., Nemani, R. & Running, S. W. A generalized, bioclimatic index to predict foliar phenology in response to climate. *Glob. Change Biol.* **11**, 619–632 (2005).
51. Piao, S. et al. Characteristics, drivers and feedbacks of global greening. *Nat. Rev. Earth Environ.* **1**, 14–27 (2020).
52. Abatzoglou, J. T., Williams, A. P. & Barbero, R. Global emergence of anthropogenic climate change in fire weather indices. *Geophys. Res. Lett.* **46**, 326–336 (2019).

53. Jain, P., Castellanos-Acuna, D., Coogan, S. C., Abatzoglou, J. T. & Flannigan, M. D. Observed increases in extreme fire weather driven by atmospheric humidity and temperature. *Nat. Clim. Change* **12**, 63–70 (2022).
54. Van Wagner, C. *Development and Structure of the Canadian Forest Fire Weather Index System*. (1987).
55. Van Wagner, C. & Pickett, T. *Equations and FORTRAN Program for the Canadian Forest Fire Weather Index System*. (1985).
56. Jiménez-Ruano, A., Rodrigues Mimbrero, M. & de la Riva Fernández, J. Exploring spatial–temporal dynamics of fire regime features in mainland Spain. *Nat. Hazards Earth Syst. Sci.* **17**, 1697–1711 (2017).
57. Wotton, B. M., Flannigan, M. D. & Marshall, G. A. Potential climate change impacts on fire intensity and key wildfire suppression thresholds in Canada. *Environ. Res. Lett.* **12**, 095003 (2017).
58. Rodrigues, M., Alcasena, F. & Vega-García, C. Modeling initial attack success of wildfire suppression in Catalonia, Spain. *Sci. Total Environ.* **666**, 915–927 (2019).
59. San-Miguel-Ayanz, J., Moreno, J. M. & Camia, A. Analysis of large fires in European Mediterranean landscapes: Lessons learned and perspectives. *Ecol. Manag.* **294**, 11–22 (2013).
60. Podschwit, H. & Cullen, A. Patterns and trends in simultaneous wildfire activity in the United States from 1984 to 2015. *Int. J. Wildland Fire* **29**, 1057–1071 (2020).
61. McGinnis, S. et al. Future regional increases in simultaneous large Western USA wildfires. *Int. J. Wildland Fire* **32**, 1304–1314 (2023).
62. Damoah, R. et al. A case study of pyro-convection using transport model and remote sensing data. *Atmos. Chem. Phys.* **6**, 173–185 (2006).
63. Campos, C., Couto, F. T., Filippi, J.-B., Baggio, R. & Salgado, R. Modelling pyro-convection phenomenon during a mega-fire event in Portugal. *Atmos. Res* **290**, 106776 (2023).
64. Peterson, D. A. et al. The 2013 Rim Fire: Implications for predicting extreme fire spread, pyroconvection, and smoke emissions. *Bull. Am. Meteorol. Soc.* **96**, 229–247 (2015).
65. Peterson, D. A. et al. Wildfire-driven thunderstorms cause a volcano-like stratospheric injection of smoke. *Npj Clim. Atmos. Sci.* **1**, 1–8 (2018).
66. Fromm, M., Servranckx, R., Stocks, B. J. & Peterson, D. A. Understanding the critical elements of the pyrocumulonimbus storm sparked by high-intensity wildland fire. *Commun. Earth Environ.* **3**, 1–7 (2022).
67. Fromm, M. et al. The untold story of pyrocumulonimbus. *Bull. Am. Meteorol. Soc.* **91**, 1193–1210 (2010).
68. Potter, B. E. Atmospheric interactions with wildland fire behaviour–II. Plume and vortex dynamics. *Int. J. Wildland Fire* **21**, 802–817 (2012).
69. McRae, R. H., Sharples, J. J. & Fromm, M. Linking local wildfire dynamics to pyroCb development. *Nat. Hazards Earth Syst. Sci.* **15**, 417–428 (2015).
70. Dowdy, A. J., Fromm, M. D. & McCarthy, N. Pyrocumulonimbus lightning and fire ignition on Black Saturday in southeast Australia. *J. Geophys. Res. Atmospheres* **122**, 7342–7354 (2017).
71. Peterson, D. A. et al. Australia's Black Summer pyrocumulonimbus super outbreak reveals potential for increasingly extreme stratospheric smoke events. *Npj Clim. Atmos. Sci.* **4**, 1–16 (2021).
72. Bedia, J. et al. Global patterns in the sensitivity of burned area to fire-weather: Implications for climate change. *Agric. Meteorol.* **214**, 369–379 (2015).
73. El Garroussi, S., Di Giuseppe, F., Barnard, C. & Wetterhall, F. Europe faces up to tenfold increase in extreme fires in a warming climate. *Npj Clim. Atmos. Sci.* **7**, 1–11 (2024).
74. Tejedor, E. et al. Recent heatwaves as a prelude to climate extremes in the western Mediterranean region. *Npj Clim. Atmos. Sci.* **7**, 1–7 (2024).
75. Serrano-Notivoli, R. et al. Unprecedented warmth: A look at Spain's exceptional summer of 2022. *Atmos. Res* **293**, 106931 (2023).
76. Büntgen, U. et al. Recent summer warming over the western Mediterranean region is unprecedented since medieval times. *Glob. Planet. Change* **232**, 104336 (2024).
77. Brotons, L., Aquilué, N., de Cáceres, M., Fortin, M.-J. & Fall, A. How fire history, fire suppression practices and climate change affect wildfire Regimes in Mediterranean Landscapes. *PLOS ONE* **8**, e62392 (2013).
78. Moreno, M. V., Conedera, M., Chuvieco, E. & Pezzatti, G. B. Fire regime changes and major driving forces in Spain from 1968 to 2010. *Environ. Sci. Policy* **37**, 11–22 (2014).
79. Ruffault, J. & Mouillot, F. How a new fire-suppression policy can abruptly reshape the fire-weather relationship. *Ecosphere* **6**, art199 (2015).
80. Cunningham, C. X., Williamson, G. J. & Bowman, D. M. J. S. Increasing frequency and intensity of the most extreme wildfires on Earth. *Nat. Ecol. Evol.* **8**, 1420–1425 (2024).
81. Vicedo-Cabrera, A. M., Esplugues, A., Iñíguez, C., Estarlich, M. & Ballester, F. Health effects of the 2012 Valencia (Spain) wildfires on children in a cohort study. *Environ. Geochem. Health* **38**, 703–712 (2016).
82. Cascio, W. E. Wildland fire smoke and human health. *Sci. Total Environ.* **624**, 586–595 (2018).
83. Pacheco, R. M. & Claro, J. Characterising wildfire impacts on ecosystem services: a triangulation of scientific findings, governmental reports, and expert perceptions in Portugal. *Environ. Sci. Policy* **142**, 194–205 (2023).
84. Nunes, J. P. et al. Afforestation, Subsequent Forest Fires and Provision of Hydrological Services: a Model-Based Analysis for a Mediterranean Mountainous Catchment. *Land Degrad. Dev.* **29**, 776–788 (2018).
85. Moritz, M. A. et al. Learning to coexist with wildfire. *Nature* **515**, 58–66 (2014).
86. McWethy, D. B. et al. Rethinking resilience to wildfire. *Nat. Sustain.* **2**, 797–804 (2019).
87. Hersbach, H. et al. The ERA5 global reanalysis. *Q. J. R. Meteorol. Soc.* **146**, 1999–2049 (2020).
88. Riahi, K. et al. The shared socioeconomic pathways and their energy, land use, and greenhouse gas emissions implications: an overview. *Glob. Environ. Change* **42**, 153–168 (2017).
89. Meinshausen, M. et al. The shared socio-economic pathway (SSP) greenhouse gas concentrations and their extensions to 2500. *Geosci. Model Dev.* **13**, 3571–3605 (2020).
90. Lawrence, D. M. et al. The Land Use Model Intercomparison Project (LUMIP) contribution to CMIP6: rationale and experimental design. *Geosci. Model Dev.* **9**, 2973–2998 (2016).
91. Rothermel, R. C. *A Mathematical Model for Predicting Fire Spread in Wildland Fuels*. (1972).
92. Nelson Jr, R. M. Prediction of diurnal change in 10-h fuel stick moisture content. *Can. J. Res.* **30**, 1071–1087 (2000).
93. Carlson, J. D., Bradshaw, L. S., Nelson, R. M., Bensch, R. R. & Jabrzemski, R. Application of the Nelson model to four timelag fuel classes using Oklahoma field observations: model evaluation and comparison with National Fire Danger Rating System algorithms. *Int. J. Wildland Fire* **16**, 204–216 (2007).
94. Yebra, M. et al. Globe-LFMC, a global plant water status database for vegetation ecophysiology and wildfire applications. *Sci. Data* **6**, 155 (2019).
95. Aragoneses, E., García, M., Salis, M., Ribeiro, L. M. & Chuvieco, E. Classification and mapping of European fuels using a hierarchical, multipurpose fuel classification system. *Earth Syst. Sci. Data* **15**, 1287–1315 (2023).
96. Scott, J. H. & Burgan, R. *Standard Fire Behavior Fuel Models: A Comprehensive Set for Use with Rothermel's Surface Fire Spread Model*. (2005).
97. Brogli, R., Heim, C., Mensch, J., Sørland, S. L. & Schär, C. The pseudo-global-warming (PGW) approach: methodology, software package PGW4ERA5 v1. 1, validation, and sensitivity analyses. *Geosci. Model Dev.* **16**, 907–926 (2023).
98. Schär, C., Frei, C., Lüthi, D. & Davies, H. C. Surrogate climate-change scenarios for regional climate models. *Geophys. Res. Lett.* **23**, 669–672 (1996).

Acknowledgements
Funding comes from the Spanish Ministry of Science and Innovation RIESPIRO (PID2021-128510OB-100) and the CRETUS strategic partnership (AGRUP2015/02), co-funded by the European Union ERDF. This work was supported by the project 'Climate and Wildfire Interface Study for Europe (CHASE)' under the 6th Seed Funding Call by the European University for Well-Being (EUniWell). MSR acknowledges Xunta de Galicia for a predoctoral grant (Programa de apoio á etapa predoutoral 2019, ED481A-2019/112). DIC acknowledges support from the European Research Council (HEAT, 101088405). Computation took place at CESGA (Centro de Supercomputacion de Galicia), Santiago de Compostela, Galicia, Spain.

Author contributions
M.S.R. designed the study, performed the analysis, created the figures and drafted the manuscript. D.I.C. and G.M.M. provided critical feedback and contributed to writing the paper.

Competing interests
The authors declare no competing interests.

Additional information
Supplementary information The online version contains supplementary material available at https://doi.org/10.1038/s41612-025-00906-3.

Correspondence and requests for materials should be addressed to Martín Senande-Rivera.